Mapping the A-team at the X-band: an evolving group of radio-loud multi-spectral objects

Berkeley Radio Lab

University of California Berkeley

Using an interferometer consisting of two parabolic reflectors several celestial sources have been observed in the X*-band* (10.5 GHz). *After a short review of the history and theory of radiometric interferometry is given, the methods of relative flux calibration for radio astronomy are used—with the brightest radio sources in the sky, the "A-team"*[1]—Virgo A (M87), Taurus A (M1, *a.k.a.* The Crab Nebula), Cassiopeia A, and Cygnus A—*to find the gain, system temperature, and antenna temperature of the Campbell Hall Analog Kaleidoscopic Radio Array* (CHAKRA) *located on the roof of Campbell Hall. Next, horizon-to-horizon data from both the Sun and moon are used to measure the baseline of the interferometer* ($\sim$ 15m) *in the spirit of similar geophysical measurements. The angular resolution provided by this baseline* ($\sim 5'$) *along with the* uv*-plane coverge of* CHAKRA *is then used to present both standard—typically an automatic computer algorithm—and non-standard (i.e., manual) imaging processes.*

1 Introduction: radio interferometry

Interference effects, from wave mechanics, are found across the entire electromagnetic spectrum. Radio astronomy, using wavelengths in the range of a few millimetres to many meters, uses these effects to "synthesize" larger telescopes, from a few meters up to the size of the earth by interferometry. In the past, radio telescopes had a much lower resolution than optical telescopes. Today, radio telescopes offer unsurpassed resolution,[2] partly because building interferometers with visible light is extremely hard; the largest interferometers do not use wires to construct baselines, they use post-processing requiring very high precision timing (e.g., atomic clocks and hydrogen masers). This Very Long Baseline Interferometry (VLBI), with (sub-)μ-arcsecond angular resolution, can be used to measure crustal dynamics of the Earth, astrophysical masers, and the edge of black holes.

The arrival of radio astronomy, in the 1930s, was followed a few years later by discrete sources in radio maps made by Grote Weber. Then, in the 1950s, the epochal 21cm line of hydrogen was detected along with radio bursts from the sun. The next decade brought the discovery of quasars, pulsars, and the cosmic microwave background (CMB) along with the advent of aperture synthesis by Martin Ryle [Hew65]; initially, interferometry was hobbled

[1] Not to be confused with the former special forces operatives in the popular TV show *The A-team*. When this show first aired in 1983 it would have been broadcast in the VHF band (see Figure 3).

[2] Working alone (high sensitivity) they can detect a "cell phone call from Jupiter," working together (high resolution) they can see a "penny on the moon" [Wol08].

by a lack of computer power to perform Fourier transforms, this changed in the 1970s with increasing computing power. In the 1980s, the Jansky Very Large Array (JVLA) in New Mexico was constructed which then became a part of the Very Large Baseline Array (VLBA) in the 1990s. In the past twenty years, smaller wavelength observatories and a colossal radio telescope, e.g., the Atacama Large Millimetre/submillimetre Array (ALMA) and the Five-hundred-meter Aperture Spherical Telescope (FAST), were constructed with the sensitivity to see protoplanetary disks and (potentially) extraterrestrial signals; however, the main push seems to towards large-scale interferometry, i.e., very long baseline interferometry (VLBI), and highly sensitive radio telescopes with a large effective collecting area from small baseline interferometry in regions with low radio interference (signals from terrestrial sources) to view the universe before reionization took place.[3]

Interferometers were first used by Michelson in an attempt to measure the absolute motion of the earth with respect to the aether by seeing a shift in fringe patterns. Radio interferometers also generate fringe patterns as an output; conversely, they can be seen as projecting an interference pattern onto the sky (see Figures 1 and 2). The sky itself has a brightness temperature T_B as measured by the individual antennas $I(\theta, \phi)$ with their beam patterns $A(\theta, \phi)$; the interferometer allows astronomers to effectively sample a Fourier transform of the sky's brightness temperature T_B when the signals are in someway added or multiplied (see Figure 2). The thing being sampled is what radio astronomers call the ***visibility*** with oscillating ***fringes***, when $A(\theta, \phi)$ and $I(\theta, \phi)$ are projected into the (x, y) plane it is

$$V(u, v) = \int\int A(x, y)I(x, y)e^{-2\pi i(ux+vy)}dxdy \tag{1}$$

where $u\lambda = d\sin\phi = x$ and $v\lambda = d\cos\phi = y$ (note that this convention is useful because usually the antennas are moved at intervals of the wavelength to eliminate diffraction effects [Hew65]). This is essentially the contrast of the interference pattern (degree of coherence). The theory behind this mathematical apparatus is the ***van Cittert–Zernike theorem***, which says that the signals being received by the two antennas are (sort of) coherent because they have a constant phase-relation over time (they are the same modulo the geometric time delay τ_g), this coherence of incoherence makes it all work.[4]

Most astronomical sources are incoherent, like the Sun which is very well approximated as a thermal black body (Section 4). Only objects like pulsars and masers transmit temporally coherent signals. However, because of the vast distances involved in astronomy the multitude of incoherent sources get smoothed out over space—making them spatially coherent. This can be compared to the waves generated by a few stones thrown into a lake, turbulent where they enter and laminar along the shore. Just as two detectors on the shore could record the wave fronts and reconstruct the stone impacts by correlating their signals and then taking a Fourier transform—carefully taking the Fourier transform of $V(u, v)$ can yield a brightness temperature distribution $T_B(\theta, \phi)$, a map of the sky.[5]

[3]These signals are < 1 Jy, whereas a cell phone *on the moon* would produce a signal on Earth around $50,000$ Jy.

[4]There is an entire field called "Coherence Theory" and the concept is also often applied in atomic and molecular physics. Misconceptions abound on this topic (e.g., http://amasci.com/miscon/coherenc.html), however, for radio astronomy, the important concepts are time and spatial coherence [Cla89]. This can be thought of as: *how well does the source approximate a perfect, monochromatic point source*.

[5]Radio interferometers have also been used to successfully measure continental drift (also a product of the

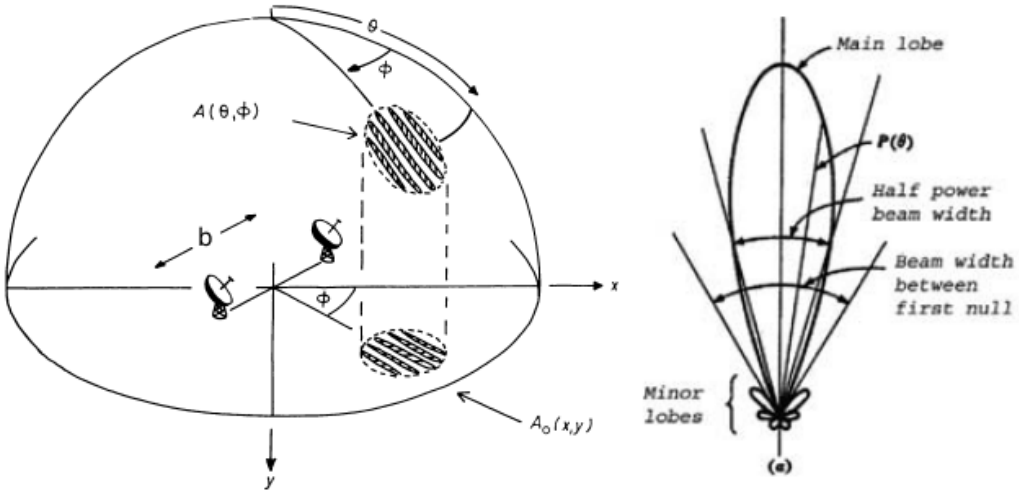

Figure 1: *Schematic of a two element radio interferometer (left) [Hew65] and beam pattern (right) [Che10]. A simplified baseline is typically assumed to be exactly alinged with the equator E-W without a N-S component.*

2 Methods

The interferometer on the roof of Campbell hall has a single baseline, b, that is approximately 15 meters along the E-W axis with a small N-S component (see Figure 5). This is smaller than any single dish (there are 28) of the JVLA (~ 25 m). Unlike larger, additive arrays that correlate baselines digitally in post-processing this array, which spins kaleidoscopically in the uv-plane, has an analog multiplicative correlator—accordingly, this telescope will be referred to as the Campbell Hall Analog Kaleidoscopic Radio Array (CHAKRA). The two antennae of CHAKRA are housed in feed horns collecting 10.5 GHz (2.855 cm) radio waves at the focus of $r = 0.457$ m parabolic reflectors; these are single polarization feeds so a conservative (with respect to error) antenna efficency factor $\eta_{IQUV} = .5 \pm .25$ will be used for all measurements [RH18]. The resolution of this "synthesized" aperture is roughly $\theta \approx \lambda/b \approx 4.816'$ (each dish would individually have $\theta \approx \lambda/2r \approx 1.756^\circ$); the actual beam geometry (because CHAKRA is only a two element array) is a projected ellipse with the the minor and major axis being the two preceeding values, respectively .

Data was collected by remotely slewing the telescope, located at **Latitude = 37.87° Longitude = -122.26°**, over Secure SHell (SSH) with an `astropy` program written to track the targets using electronic stepper motors as a drive system on alt-az mounts. An in depth description of the entire signal chain is beyond the scope of this report; however, the bandwidth of the telescope is 2 MHz—making the power received $P = A(\theta,\varphi)I(\theta,\varphi)\pi r^2 \Delta\nu \approx F_\nu(1.31\ \text{m}^2)(2\times 10^6\ \text{Hz})$, where F_ν is the incident flux modulo the beam pattern.[6]

60s), the rotation rate of the Earth, and the wobble of the Earth's axis. This methodology is also similar to x-ray diffraction in condensed matter physics where a 2D interference pattern, the *reciprocal lattice*, is the Fourier transform of the crystal lattice.

[6]There is a trade-off when determining the bandwidth: while a larger bandwidth increases power, it can introduce *bandwidth smearing*. There is also considerations of *time smearing* [JM15]. These types of relations are common in signal analysis as in the uncertianly relation of Fourier transforms and quantum mechanics. For a complete schematic diagram of the signal chain, see: `https://github.com/AaronParsons/ugradio/blob/master/lab_`

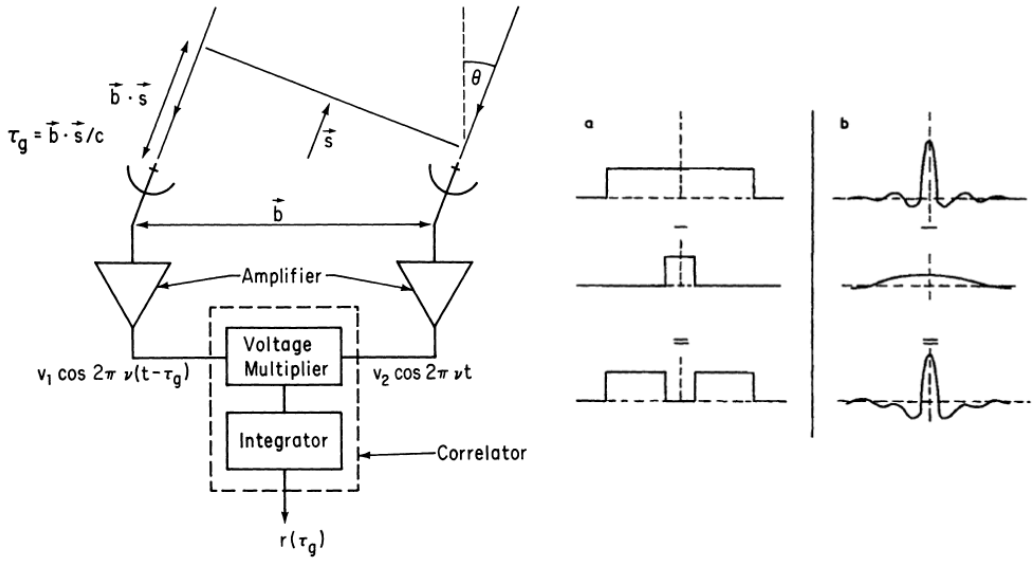

Figure 2: *Schematic picture of a two element radio interferometer [Tho99] (left). Flux calibration of interferometer shown pictorially (right). The (a) panel shows the Fourier transform of the (b) panel which is analogous to a fringe pattern (i.e., synthesized beam) with sidelobes on top and a simplified gaussian beam patten in the middle—the superposition is the bottom [BW85]. Sometimes a single, smaller dish can be incorporated into a larger array to minimize this effect.*

Source	**Distance**	**Angular Size**	Ω_S	**Size**	**Beams** B_Ω	**Object**	M_v	$M_\odot$	α
Cassiopeia A	3.40 kpc	$3.15' \times 3.5'$	2.09×10^{-6}	~ 10 ly	$1.3 \pm .25$	SNR	$+11 >$	$\gtrsim 3$	$\sim .7$
Cygnus A	232 Mpc	$0.56' \times 1.19'$	1.27×10^{-7}	~ 100 kpc	$\lesssim 1$	AGN	$+16.22$	1×10^{14}	$\lesssim 0$
Taurus A	1.99 kpc	$2.8' \times 4.06'$	2.16×10^{-6}	~ 1.7 pc	$1.05 \pm .25$	SNR	$+8.4$	1.4	$\sim .3$
Virgo A	16.4 Mpc	$0.7' \times 1.4'$	1.86×10^{-7}	~ 100 kpc	$2.5 \pm .25$	AGN	$+8.79$	7×10^9	$\gtrsim 0$
Zenith	$[0, \infty)$	$\sim 2\pi$	2π	–	–	–	–	–	2

Table 1: *Important figures for the A-team sources. Size is the major axis if objects are elongated. "Beams" is beams per source (the beam packing B_Ω), which is related to the brightness/flux sensitivity by the aperature efficency $\eta = A_0/A = 2k_B T_A/S_\nu A$, where T_A is the antenna temperature $T_A = T_B(\Omega_S/\Omega_A)$, Ω_S is the angular size of the source (solid angle subtended), $\Omega_A = \int\int_{Sky} A(\theta,\phi)d\Omega \approx 3.1 \pm 2 \times 10^{-6}$ is the solid angle of the beam, S_ν is the flux density, A_0 is the effective collecting area, and A is the physical collecting area [PM05]. The beam packing quantifies the antenna temperature and enables the determination of brightness sensitivity set by the ratio of antenna to brightness temperature. The kilokelvin system temperature (see Table 3) is mostly antenna temperature, making CHAKRA's sensitivity low and requiring long integrations and/or a bright source for high-contrast imaging. SNR is SuperNova Remenant and AGN is Active Galactic Nuclei. M_v is the apparent bolometric magnitude, $M_\odot$ is the mass in solar units, and α is the (generalized) spectral index [Gre19]. The expected number of beams for Virgo A was $\gg 1$ (see Figure 5) however it is likely only the jet was able to saturate the feed, which only has one polarization. (Most jets are known to be polarized.) Interestingly, Cygnus A was resolvable into two blob-like sources; see Section 4 for more.*

There are basically two options for a two element array: additive or multiplicative [BGS09].[7] CHAKRA utilizes the multiplicative approach, which benefits from reduced noise. Signals from the two antennae are sent to a *correlator* that effectively multiplies them, turning voltages into power. The following equation is a version of Equation 1 cast as the output in Figure 2, i.e., the response, $\mathcal{R}(\tau_g)$, of the array [JM15]:

$$\mathcal{R}(\tau_g) = \langle E_1 \cdot E_2 \rangle = \frac{E_0^2}{2} \cos\left(2\pi \frac{b}{\lambda} \sin \omega_E t\right) \tag{2}$$

where E_1 is the signal from one antenna, E_2 the signal from the other antenna, and $\omega_E = 7.29 \times 10^{-5}$ radians s^{-1} is the rotation of the earth; the averaging on the left side indicates that any noise in the signals will, after a sufficiently long integration time, go to zero.[8] In order to calibrate CHAKRA, it was necessary to determine the amplitude term $E_0^2/2$ by observing a source with a known absolute flux density and then matching it with the response $\mathcal{R}(\tau_g)$.

Typically, it is very hard to determine the absolute flux (read: gain) of an interferometer by theoretical means. For single pyramidal horn telescopes this is possible—so they are typically used to measure absolute flux density of a good reference source, which can then be used to calibrate larger interferometers.[9] It is desirable for a reference source to be a bright and stable point source[10]; two of the most important from the literature are Cygnus A and Virgo A (M87) [Baa14]. These are both "radio galaxies," strong synchrotron radiation emitters powered by supermassive black holes—making them stable over long timescales and non-thermal sources (bright at low frequencies).[11] A horizon-to-horizon observation of both these sources was conducted.

These are both nearly point sources for CHAKRA (see Table 1). The response data was processed by removing any bias introduced from the signal chain, averaged, and then squared to retrieve the root mean square (RMS) voltage—this could then be multiplied by $\sqrt{2}$ to get the peak voltage V_P of the fringe. Once this was found, it was used to calibrate the response of CHAKRA as the gain could be found by dividing V_P by the known absolute flux density (after subtracting the zenith V_{rms}). The measurement results are presented in Table 2, along with the absolute values from the power law functions used to generate the flux den-

`interf/interf_signal_path.pdf`.

[7] A multiplicative interferometer is also called a *cross-correlation interferometer*. The visibility/fringe is technically a complex function (see Equation 1), however for CHAKRA the output was only real values. It is possible to get both real and imaginary parts with a more complex correlator [Hew65][JM15].

[8] The gauge for zero is often hard to find for interferometers. Multiplicative interferomters theoretically avoid the zero spacing problem and should actually average to zero in the limit of long integrations. However, with additive synthesis, a negative "basin" often appears in the product (see right side of Figure 2) because the zero spacing is missing; this means multiplicative interferometers could be better at resovling large scale structure and getting better (relative) flux measurements.

[9] The parabolic dishes typically used to construct interferometers have much bigger sidelobes in the beam pattern than horns. Moreover, the response of the entire interferometer is more complicated than a single parabolic dish. Interestingly, the horn reflector used by Penzias and Wilson, which detected the Cosmic Microwave Background (CMB), was special built to make the sidelobes as small as possible.

[10] A point source makes sure the fringe amplitude is constant (the Fourier transform of a point is a constant).

[11] It is fortuitous that non-thermal sources are actually brighter at larger wavelengths, where it is easier to manage noise along with other technological considerations, unlike thermal sources. Cygnus A was discovered by Grote Weber in 1939 observing radio waves in the very high frequency (VHF) band at 160 MHz (1.9 m).

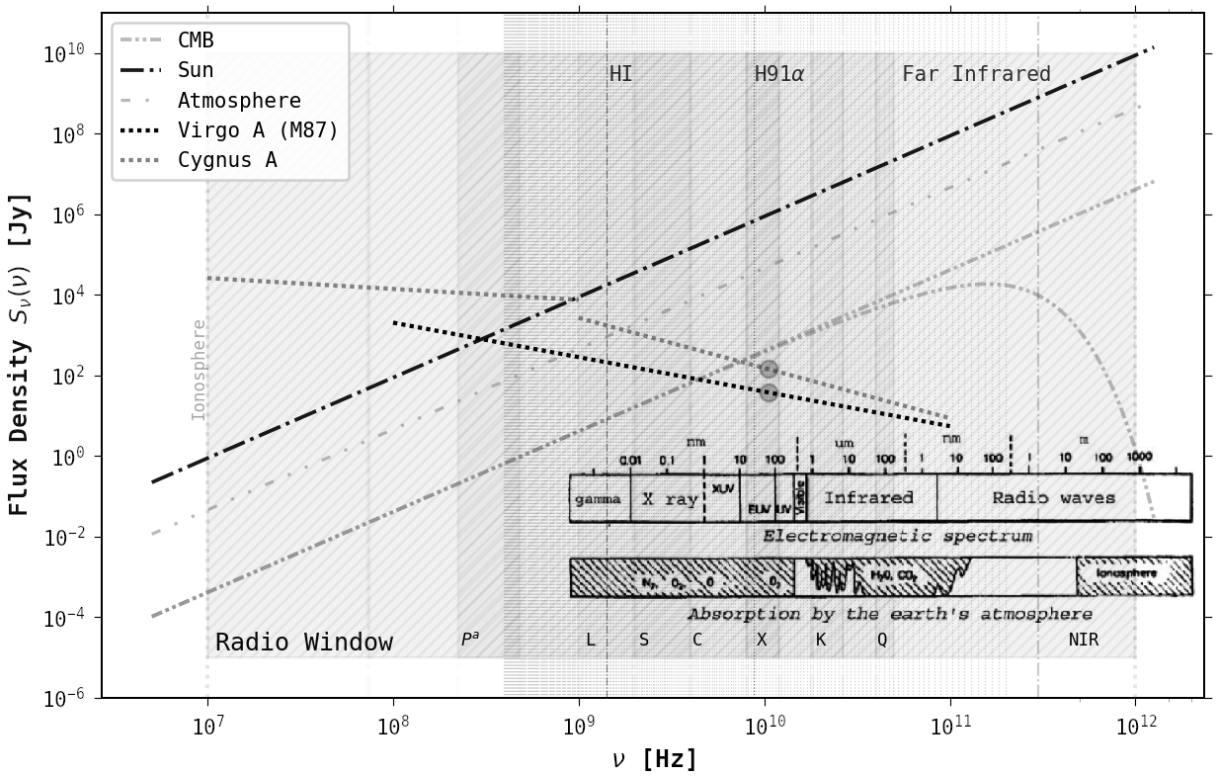

Figure 3: *Spectral energy distribution plot showing thermal (postive slope with $\alpha \sim 2$) and non-thermal sources (negative slope). The Rayleigh-Jeans continuation is shown for the CMB—the approximation appears to hold for the X-band and will be used throughout this paper. A temperature of 300, 2.7, and 5777 K was used for the atmosphere, CMB, and Sun, respectively. Radio hydrogen recombination lines related to HII regions are shown from $n = 256$ to $n = 32$ along with the HI line. The HF (3-30 MHz), VHF (30-300 MHz), and UHF (300 MHz to 1 GHz) bands used for FM/AM radio, TV, and other communciations would be indicated where the text "Radio Window" is found. Note that the HF band goes outside of the radio window. Ham radio operators, who operate in this band, have used the ionosphere to bounce transmissions around the Earth—like on the expedition of the Kon Tiki [FL57]. Inset found in [Che10].*

sity spectrum.[12] With the assumption of Cygnus A being a point source the gain factor for CHAKRA was found to be $G_{Jy} = 2.07 \times 10^{-9}$ V^2/Jy$\cdot$Beam; the conversion factor for brightness temperature T_B is then $G_K = 3.40 \times 10^{-7}$ K/Jy. Source fringes were shifted in a non-linear way by ~ 1100 K above zenith, which included galactic background and the CMB, enabling an approximate solution for system temperature (this calibration technique is similar to a "hot-cold-load" [Baa14]; see Table 3 for full breakdown).

3 The A-team: supernova remnants and radio galaxies

The brightest star in a constellation is typically given the designation α, however, for (non-thermal) radio sources, which are often dim in the optical band, the appelation "A" is used.

[12]These power laws are of the form: $\log_{10} S_\nu = a + b \log_{10} \nu + c \log_{10}^2 \nu$ (a, b, and c are called *spectral parameters*).

Source	Frequency Range	a	b	c	$S_{Abs}(\nu)$	V_p	$S_{Rel}(\nu)$	$(S_{Rel}+\beta)\cdot B_\Omega$
Cassiopeia A	$22-300$ MHz	5.625	-0.634	-0.023				
	$300-31$ GHz	5.880	-0.792	–	488.35*	6.7×10^{-7}	321.5	488.15
Cygnus A	$20-2$ MHz	4.695	$+0.085$	-0.178				
	$2-31$ GHz	7.161	-1.244	–	140.75	5.8×10^{-7}	140.8	–
Taurus A	$1-35$ GHz	3.915	-0.299	–	513.11*	9.0×10^{-7}	434.5	512.9
Virgo A	400 MHz – 25 GHz	5.023	-0.856	–	37.48	8.0×10^{-8}	-38.47	38.825
Zenith	10.5 GHz	–	2	–	–	1.3×10^{-6}	630.9	684.9

Table 2: *A-Team absolute and relative flux density at $\nu = 10.5$ GHz [Jy] and spectral parameters [Baa14]. The method used to obtain V_p is described in Section 2. The relative flux density for Cygnus A (the most point-like source) is taken to be a single beam, the other sources are larger and so the beam packing can be solved for (see Table 1). Variations in the atmosphere and sky complicate an absolute flux density for the zenith, typically with large additive arrays calibration pointings near the target will be taken on a regular basis. The negative basin is apparent in the values; linear regression across the A-team yielded a basin of $\beta \sim 54$ Jy, which was used to re-solve for B_Ω (see Table 1). *Secular variations not included.*

The brighest such radio source in the sky is Saggitarius A, found by Carl Jansky during his epochal radio survey. On the heels of this discovery of "cosmic static" Grote Reber set out to test if the source was thermal by measuring at higher frequencies where a thermal, blackbody source would have much higher flux. The null result Reber's work turned up was later explained by Shklovsky's theory of synchrotron radiation [BVK85]. Reber's higher freqency rig using a parabolic reflector dish with higher directional gain—and correspondingly higher resolution map—was able to resolve Cygnus A (see Figure 4).

After World War II a smörgåsbord of radar equipment was repurposed for radio astronomy [FoGB10]. Higher resolution was achieved with larger dishses, oceanic interferometry, and eventually interferometric arrays. More complicated telescopes required better calibrations and the four brightest discrete sources—the A-team consisting of Virgo A (M87), Taurus A (M1, *a.k.a.* The Crab Nebula), Cassiopeia A, and Cygnus A—become the go-to calibrators. This group has two supernovae rements and two radio galaxies and happens to be a great sample of radio-loud objects. Radio source catalogs grew over the years and the highest resolution radio telecopes began requiring smaller, point-like calibrators (e.g., planets and quasars) but the A-team remains possibly the most well observed objects in the sky, at all wave bands, outside of the solar system.

Radio astronomy grew up in the shadow of Hubble's discovery of extra-galactic objects. Penzias and Wilson's accidental detection of the CMB is generally regarded as the clinching evidence in favor of big bang cosmology. Today, cosmology is typically reckoned at the scale of megaparsecs (Mpc), with the universe being considered isotropic, homogenous, and flat. On smaller scales, galaxies have been found to have "flat" rotation curves, usually attributed to dark matter. Radio astronomy can measure the velocity distribution of HI and use CO as a tracer for H_2 clouds and star forming regions.

While most young galaxies appear to have active nuceli (AGN), there are also nearby galaxies with AGN. Virgo A (M87) is located in our local group and has a jet pointed almost head on towards the Milky Way. In contrast, Cygnus A has jets almost in the plane of the sky, and is located much farther away ($\sim$ 14 times). Most resolved galaxies that are radio-loud (basically those galaxies with AGN) are generally referred to as "radio galaxies," although

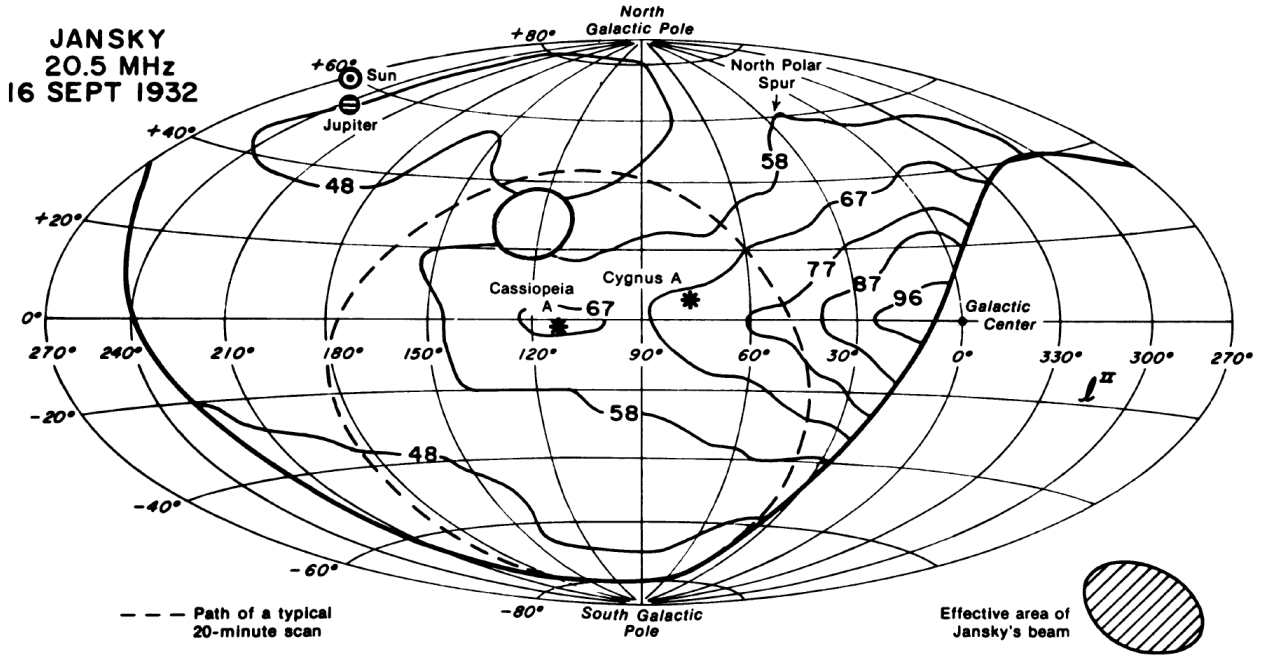

Figure 4: *An updated version of Jansky's original radio map. Contours indicate isotherms of brightness temperature in units of 1000 K (because this is non-termal radiation these values are not related to a thermal temperature). Image found in [BVK85].*

there is a smattering of terms for the variety of observable differences. These differences are likely to be due to line-of-sight effects and not intrinsic to the galaxy/AGN.

Supernovae have been implicitly known about for a long, long time. There are several types of supernovae, with the three broad categories being: massive Iron core-collapse, small Chandrasakar-triggered white dwarf, and intermediate electron-capture. Many supernova remenants are more easily viewed in radio bands and the neutron stars often found in them were first found by Anthony Hewish and Jocelyn Bell Burnell. Actually, they found pulsars, a particular type of neutron star. One of these was then almost immediately uncovered, with the late Arecibo, to be in the heart of Taurus A.

Most supernova remenants have spherical shells expanding around them. These shockwaves trace the cooling of hot gas and nuclear waste produced in the enourmous explosions. While Chandrasakar-triggered white dwarf explosions are extremely useful for cosmology they are thought to result in a thermonuclear chain-reaction that leaves little behind—no radio-loud remnants. Cassiopeia A is the youngest supernovae remeant known in the Milky Way and is moving fast on an exponential cooling curve (its flux density changes $\sim 1\,\%$ per annum) indicative of an Iron-core collapse. The neutron star remenant is not a pulsar, which could reheat the wreckage and flatten its radio spectrum with copius re-ionized free-free continuum radiation. This is precisely what is happening in Taurus A—thought to be an enigmatic electron-capture supernova—and is why it has little-to-no secular variation (neglecting glitches) and a surplus of cosmic ray high-energy particle flux.

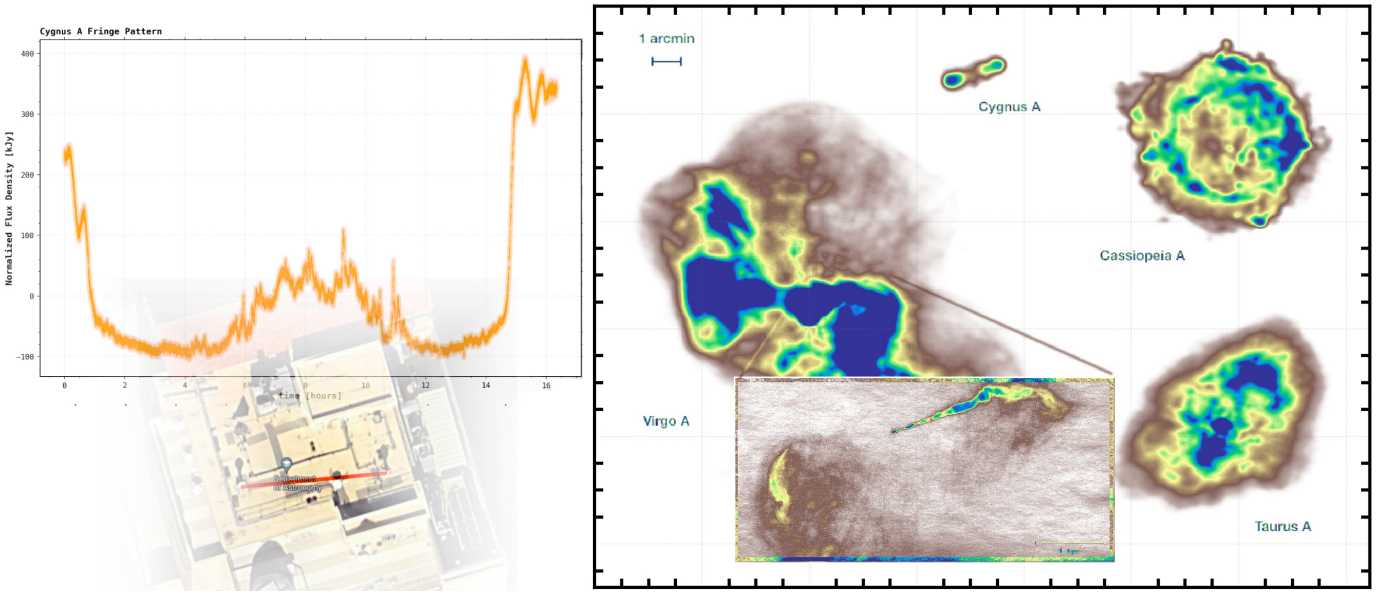

Figure 5: *Left: Cygnus A fringe pattern and CHAKRA. Right: The A-team at ultra low frequency [dGVM+20]. Virgo A (M87) is quite large, however, only the region in the inset was bright enough to be imaged [BSH91].*

4 Observations

Given the resolution of CHAKRA (and the inconsistencies of calibration) the best sources to actually observe are the Sun and moon. The Sun is the brightest radio source, emitting various types of radiation, while the moon is mostly a black body that is re-emitting radiation absorbed from the Sun as thermal radiation, like the Earth. At the time of observation, the Sun was in the middle of a lull (it was at solar minimum) and there were no Sun spots, which can usually be measured with radio telescopes. The fringe amplitude for the Sun and moon will oscillate because they are resolved sources (not point-like sources). As a non-uniform disk in the sky with limbs, sunspots, and all the rest the Sun becomes something resembling a Bessel function when a Fourier transform is performed, i.e., when it is observed with a radio interferometer (see Section 1).

The fringe pattern can be used to find the angular size of the Sun by fitting a Bessel function and assuming the Sun is a disk (cf. Figure 5); the result was less than a degree but more than several arcminutes. The Sun is typically quoted as having an angular size of $\sim .5^\circ$ because this is the angular size of the optical photosphere—the surface of last scattering for visible light. However, in the X-band, which is several decades larger in wavelength and lower in frequency, the radiation field is not as uniform and reveals more intricate structures related to non-thermal and plasma radiation processes—in the CHAKRA image the photosphere appears inside an other sphere inside a nebulous emission region. Usually interferometers rely on computers to correlate and image the raw data (visibilites) from the baselines; an outline of this process is shown in Figure 6 for Cygnus A. The uv-plane coverage can be increased by manually going through this process—with imaging software; the results are not as consistent and tend to require a model to converge on.

The starting point is taking the fringe pattern from an observation and extending it into a

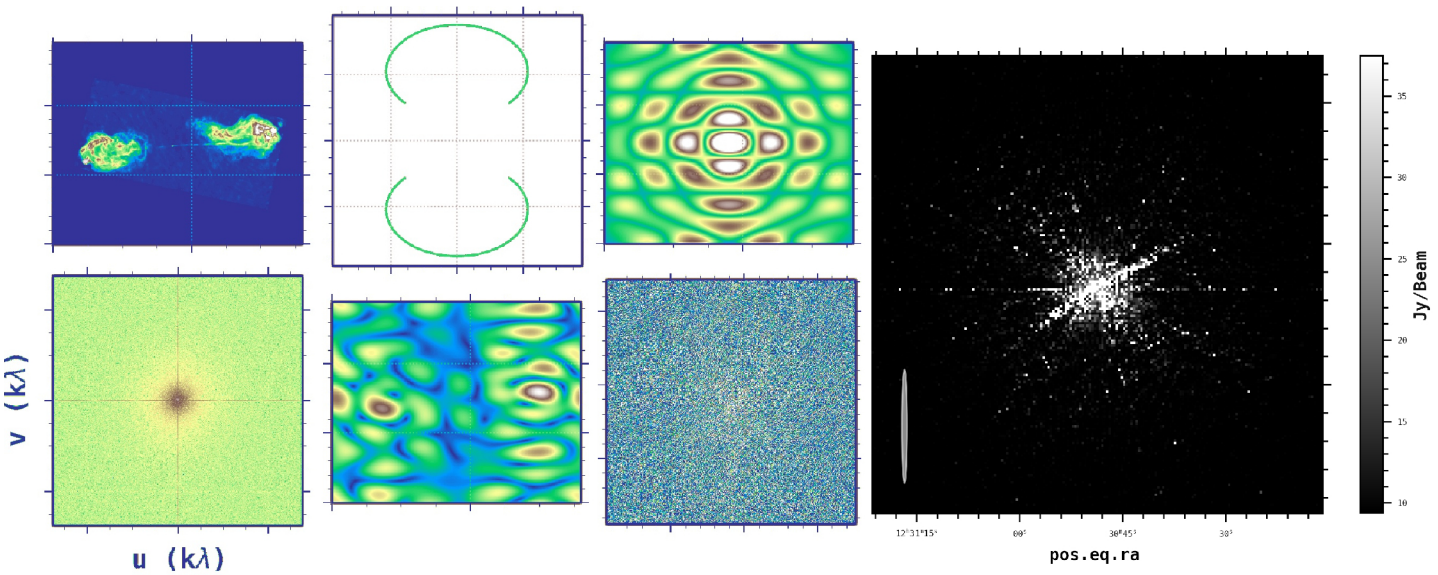

Figure 6: *On the left is an overview of uv-plane coverage of CHAKRA on Cygnus A. The model image (top left panel) is the radio map produced by the JVLA (cf. Figure 7) [PB17]. uv-plane coverage is shown in middle top panel, synthesized beam in top right, model FFT in lower left, model image in bottom middle, and actual FFT in bottom right. On the right is the clean CHAKRA image of M87. Plots generated using friendlyVRI.*

plane—generating a coherent, kaledescopic image of the fringe pattern—and then using an FFT before deconvolution; a full account of this process is beyond the scope of this report (consider it an exercise for the interested reader to manually go through the standard imaging steps and see how an image can emerge from the apparent noise). The results are shown in Figure 7 for Cygnus A. A close up of the lobes and a reference image are also provided for comparison. Applying these methods to the Sun allows for an actual representation of the Sun, warts and all, which is shown in Figure 8 along with other radio-frequency examples. The moon was similar and is omitted for brevity.

Source	**Emission Type**	**Flux Density** $S_\nu(10.5\text{ GHz})$	**Temperature**	T_B
System Temperature	Composite	183.1 kJy	–	$\sim$ 1115 K
Antenna Temperature	Johnson Noise	180.8 kJy	355+ K	$\sim$ 1100 K
Atmosphere	Thermal/Mol. Ro-Vib	1.523 kJy	$\sim$ 300 K	$\sim$ 10 K
CMB	Blackbody	443.5 Jy	2.7 K	2.456 K
Galactic Background	Synchrotron	164.2 Jy	$\gg 10^5$K	$\sim$ 1 K
HII Regions	Recombination Lines	$\sim$ 100 Jy	$> 10^4$K	$> 10^4$K

Table 3: *System components and respective temperatures. The atmosphere includes the ground (there is a lot of reflective metal on the roof of Campbell Hall). Satellite and radio transmitters, aperature effiency effects like spillover, and planets have been omitted but could be counted as an atmospheric factor.*

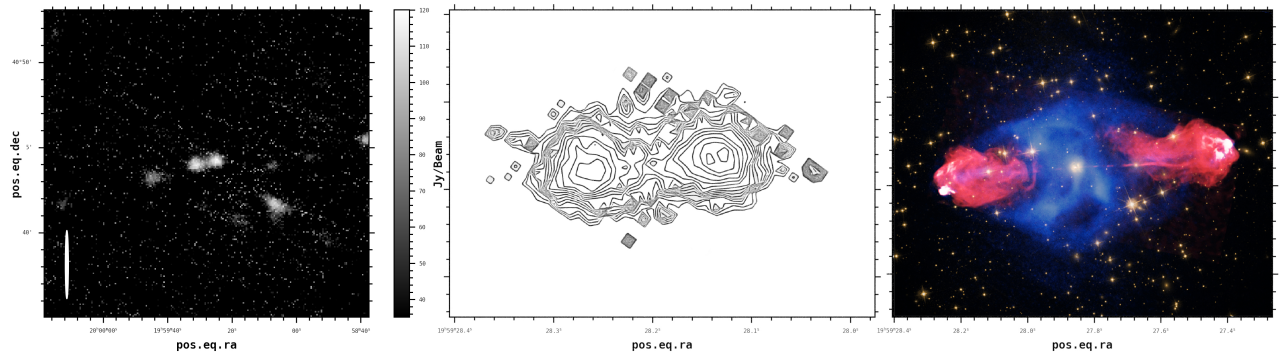

Figure 7: *Radio map of Cygnus A from CHAKRA (left), contours of the radio map (middle), and composite image including JVLA (right). For further comparison, with a 37 m single dish at 21 and 41 GHz, see [PM05]. (Credit: X-ray: NASA/CXC/SAO; Optical: NASA/STScI; Radio: NSF/NRAO/AUI/JVLA)*

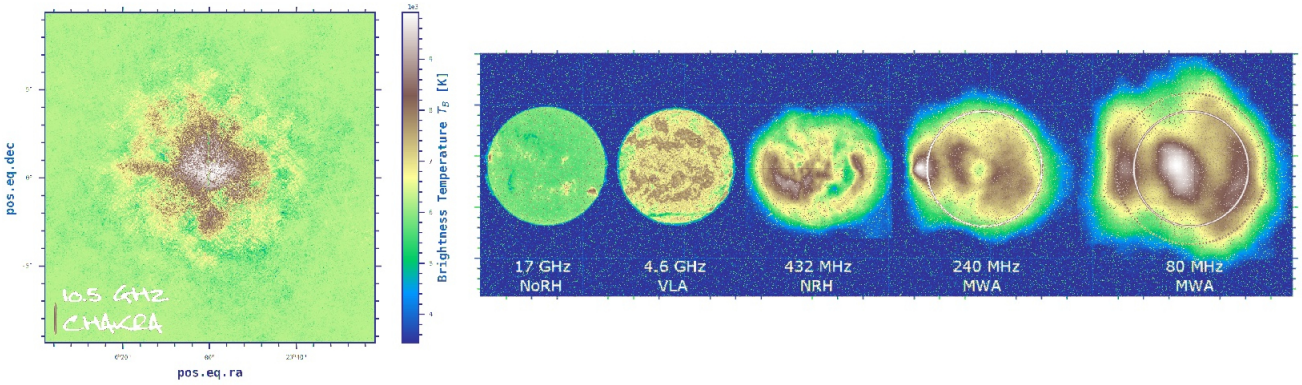

Figure 8: *CHAKRA image of the Sun at 10.5 GHz (left) and a series of images of the Sun at other radio frequencies (right): "From left to right, the observations were recorded by the Nobeyama Radioheliograph (NoRH), [Janksy] Very Large Array (JVLA), Nancay Radioheliograph (NRH), and Murchison Widefield Array (MWA). The NoRH and MWA images were taken on the same day, and the JVLA and NRH are on different days. The first two on the left are dominated by gyromagnetic emission from the chromosphere, transition region, and low-corona, while the three images on the right are dominated by thermal bremsstrahlung emission from the corona, with lower frequencies being generated at larger heights above the surface. Solid circles in the right three panels correspond to the size of the Sun seen in visible light." Image Credit:Patrick McCauley.*

References

[Baa14] J.W.M. Baars. History of Flux-Density Calibration in Radio Astronomy. *The Radio Science Bulletin*, March(348):47–66, 2014.

[BGS09] B.F. Burke and F. Graham-Smith. *An Introduction to Radio Astronomy*. Cambridge University Press, 2009.

[BSH91] J.A. Biretta, C.P. Stern, and D.E. Harris. The radio to x-ray spectrum of the m87 jet and nucleus. *The Astronomical Journal*, 101:1632, May 1991.

[BVK85] E. Bouton, G.L. Verschuur, and K.I. Kellermann. *Galactic and Extragalactic Radio Astronomy*. Astronomy and Astrophysics Library. Springer New York, 1985.

[BW85] R Braun and RAM Walterbos. A solution to the short spacing problem in radio interferometry. *Astronomy and Astrophysics*, 143:307–312, 1985.

[Che10] J. Cheng. *The Principles of Astronomical Telescope Design*. Astrophysics and Space Science Library. Springer New York, 2010.

[Cla89] Barry C. Clark. Coherence in radio astronomy. 6:1, January 1989.

[dGVM+20] F. de Gasperin, J. Vink, J. P. McKean, A. Asgekar, I. Avruch, M. J. Bentum, R. Blaauw, A. Bonafede, J. W. Broderick, M. Brüggen, and et al. Cassiopeia a, cygnus a, taurus a, and virgo a at ultra-low radio frequencies. *Astronomy & Astrophysics*, 635:A150, Mar 2020.

[FL57] P. Freuchen and D. Loth. *Peter Freuchen's Book of the Seven Seas*. Messner, 1957.

[FoGB10] J. Fielding and Radio Society of Great Britain. *Amateur Radio Astronomy*. Radio Society Of Great Britain, 2010.

[Gre19] D. A. Green. A revised catalogue of 294 galactic supernova remnants. *Journal of Astrophysics and Astronomy*, 40(4), Aug 2019.

[Hew65] A. Hewish. The synthesis of giant radio telescopes. *Science Progress*, 53(211):355–368, 1965.

[JM15] Stanley E.K. Jonathan M.M., Ronald L.S. *Fundamentals of Radio Astronomy: Observational Methods*. CRC Press, 2015.

[PB17] R. A. Perley and B. J. Butler. An Accurate Flux Density Scale from 50 MHz to 50 GHz. *The Astrophysical Journal Supplement Series*, 230(1):7, may 2017.

[PM05] P. Pratap and Gordon McIntosh. Measurement of the radiation from thermal and nonthermal radio sources. *American Journal of Physics*, 73:399–404, 05 2005.

[RH18] Timothy Robishaw and Carl Heiles. The measurement of polarization in radio astronomy. 2018.

[Tho99] A. R. Thompson. Fundamentals of Radio Interferometry. *ASP Conference Series*, 180:11–36, 1999.

[Wol08] M. Wolverton. The New Radio Sky. *Scientific American*, 299(3):18–20, 2008.